ACS OMEGA

Article

Cite This: ACS Omega 2019, 4, 5029−5037

http://pubs.acs.org/journal/acsodf

Depth Distribution of Spin-Labeled Liponitroxides within Lipid Bilayers: A Combined EPR and Molecular Dynamics Approach

Emiliano Laudadio,[†,‡] Roberta Galeazzi,[*,‡] Giovanna Mobbili,[‡] Cristina Minnelli,[‡] Antonio Barbon,[*,§] Marco Bortolus,[§] and Pierluigi Stipa[*,†]

[†]Dipartimento S.I.M.A.U. and [‡]Dipartimento di Scienze della Vita e dell'Ambiente (DISVA), Università Politecnica delle Marche, via Brecce Bianche, 60131 Ancona, Italy

[§]Dipartimento di Scienze Chimiche, Università degli Studi di Padova, Via Marzolo, 1, 35131 Padova, Italy

Supporting Information

ABSTRACT: The distribution in an egg−phosphatidylcholine bilayer of a series of spin-labeled nitroxides, potentially useful as targeted antioxidants, has been investigated using molecular dynamics (MD) simulations. The in silico method has been tested at first for a series of *n*-doxyl-phosphocholine-doped bilayers, with the doxyl moiety located at different positions (*n*) of the lipid chain, in analogy to electron paramagnetic resonance (EPR) spin labeling and other MD studies. As a result, a novel calibration curve has been obtained, suitable to determine the absolute membrane penetration depth of any paramagnetic solute from EPR measurements. A second series of MD simulations was then carried out on the newly synthesized series of liponitroxides (NOXs) recently tested as antioxidants against the lipid peroxidation of polyunsaturated fatty acids in membranes: their penetration depths, as determined by EPR in phosphatidylcholine liposomes, were correlated with their antioxidant efficacy. In these NOXs, a glycerol moiety is esterified with a carboxy derivative of a pyrroline nitroxide and one or two oleic acid residues. A very good agreement between the EPR experimental results and those from the current MD simulations indicates that the short distance of the nitroxide moiety from the fatty acid double bonds has been now definitively assessed; moreover, it indicates that our MD methodology could be successfully employed in the absence of nonparamagnetic species.

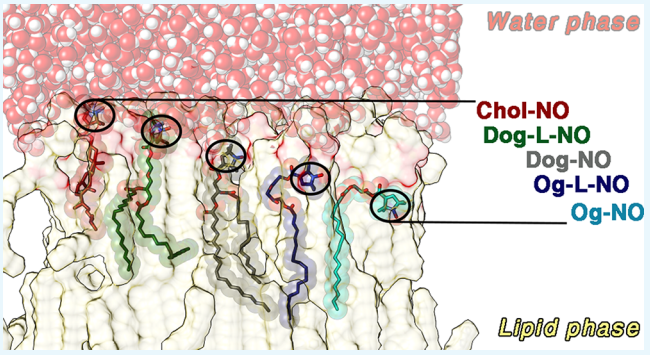

INTRODUCTION

The development of new molecules with antioxidant properties, acting specifically toward lipid peroxidation, is highly relevant in the context of medicinal, pharmaceutical, cosmetic, and food industry applications.[1−3] In fact, the oxidation of unsaturated chains, such as polyunsaturated fatty acids (PUFAs), probably represents the main damaging process that leads to the degradation of liposomal formulations in vitro and the damage of biological membranes by the production of reactive oxygen species in vivo.[4]

The compounds commonly used as antioxidants could be divided into two main classes[5] based on their mechanism of action: preventive antioxidants and chain-breaking antioxidants. Preventive antioxidants mainly inhibit peroxidative processes through the transfer of electrons to or from radical or nonradical species involved in oxidative stress, with an efficiency that depends on the redox potentials of the species involved. On the other hand, chain-breaking antioxidants directly react with the radical species involved in the oxidative chain. Nitroxides, organic stable free radicals bearing an unpaired electron mainly located in their N−O function, have proven themselves to represent very effective antioxidant species in a variety of contexts,[6−8] having the possibility to act through both the above-mentioned mechanisms. In fact, they can act as chain-breaking antioxidants for their ability to undergo fast radical−radical coupling reactions with C-centered lipid-derived radicals behaving as radical scavengers, but, at the same time, it has also been shown that the redox potentials for their reversible oxidation (in turn influenced by the molecular structure) are suitable for antioxidant properties[9−12] (see Scheme 1).

As far as biological membranes are concerned, the ability of antioxidants to be localized at specific depths, where the lipid chains are more sensitive to peroxidation, plays a key role. In this context, several newly synthesized lipid-functionalized aliphatic cyclic nitroxides (liponitroxides—NOXs, see Scheme

Scheme 1. Nitroxide Antioxidant Activity Main Mechanisms

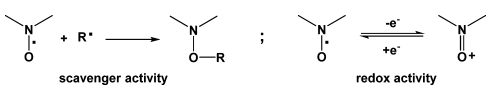

Received: December 3, 2018
Accepted: January 21, 2019
Published: March 8, 2019

DOI: 10.1021/acsomega.8b03395
ACS Omega 2019, 4, 5029−5037

Scheme 2. Structure of the Synthesized NOXs and of 5DPC[a]

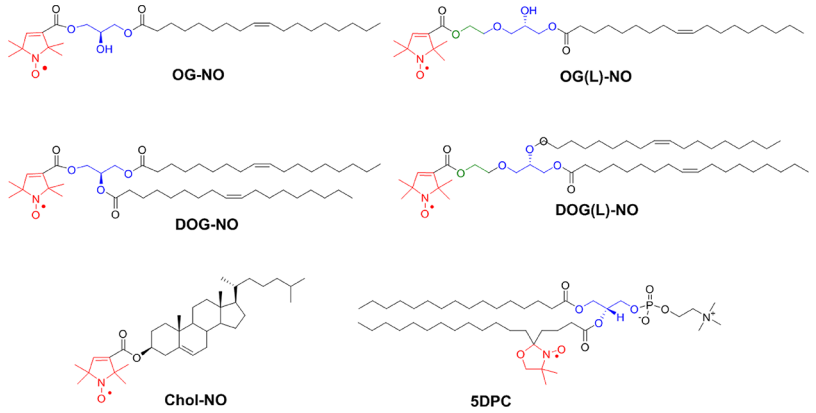

[a]In red, the nitroxide ring, in blue, the glycerol unit, and in green, the ethylene-glycol as a polar spacer.

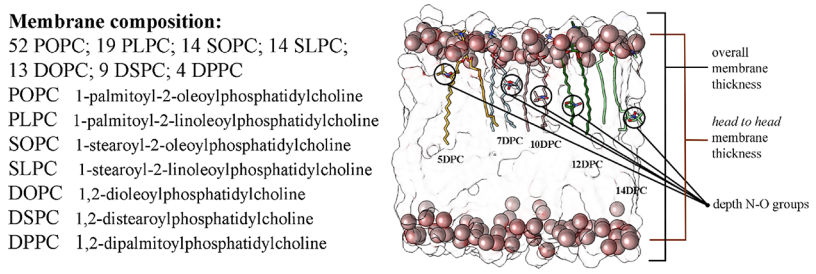

Figure 1. *n*DPCs and egg−PC membrane composition for the MD-simulated bilayers. The lipid phosphates are represented as light brown spheres for clarity and 5DPC, 7DPC, 10 DPC, 12 DPC, and 14 DPC as stick models in different colors. The N−O rings are circled to highlight their depth in the lipid membrane. The lipid matrix is reported as the transparent surface, and water and hydrogen atoms are omitted to improve the image clarity.

2) have displayed the highest activity according to their ability to localize their N−O moiety in the proximity of the PUFA double bonds in egg−phosphatidylcholine (egg−PC) liposomes, chosen as membrane models.[13] The position of the nitroxide moieties relative to the PUFAs was determined by means of spin relaxivity measurements conducted by electron paramagnetic resonance (EPR) spectroscopy.

In general, the EPR methodology is effective in providing fine information on the location and dynamics of paramagnetic antioxidants in bilayers; however, it cannot be applied to estimate the position of lipid-soluble diamagnetic antioxidant species, which is likely to influence their antioxidant power as well. In this context, molecular dynamics (MD) calculations represent an excellent methodology for a general in silico approach, which allows the prediction of the conformation, the position, and the dynamics of any molecule in a bilayer.[14] From a practical point of view, the screening of the position of designed antioxidant molecules in the membrane, before a synthetic effort takes place, is highly desirable. Moreover, the recent developments in the methodological approach used in these calculations[15] allow MD to reliably test different bilayer compositions, as, for example, inner mitochondrial membranes rich in cardiolipin, as well as membranes with different compositions;[16−19] such a feature is useful for a screening of antioxidants targeted toward different biological structures and also for supporting the EPR measurements, by creating a suitable dataset to build the calibration curve for an absolute depth determination in different biomimetic membranes where experimental data are missing.

In the present work, we produced at first a new type of calibration curve in order to obtain the absolute depth of different reference nitroxides inside the membrane (spin-labeled phospholipids) exploiting MDs calculations. Then, MD simulations on the NOXs for which the antioxidant property was tested in our previous work[13] have been carried out. The values obtained from these simulations were compared with those arising from EPR measurements.

METHODS

Setting up the Simulation Model and MD Simulation.

A membrane bilayer system consisting of 128 fully hydrated lipids was built. The bilayer was formed by lipids with a composition suited to mimic that of egg−PC:[20] 52 POPC; 19 PLPC; 14 SOPC; 14 SLPC; 13 DOPC; 9 DSPC; 4 DPPC. POPC 1-palmitoyl-2-oleoylphosphatidylcholine; PLPC 1-palmitoyl-2-linoleoylphosphatidylcholine; SOPC 1-stearoyl-2-oleoyl phosphatidylcholine; SLPC 1-stearoyl-2-linoleoylphosphatidylcholine; DOPC 1,2-dioleoylphosphatidylcholine; DSPC 1,2-distearoylphosphatidylcholine; DPPC 1,2-dipalmitoylphosphatidylcholine. Throughout this work, this mixture will be referred to as egg−PC. Finally, three molecules of spin labels [either *n*-doxyl-phosphocholine-doped bilayers (*n*DPCs) or NOXs, 3% in the mixture] were added substituting randomly pre-equilibrated PC lipids to reproduce the labeling percentage of samples used to perform EPR experiments.[13] In Scheme 2, the structures of the NOXs are reported together with a commercially available labeled phospholipid *n*DPC, where *n* indicates the carbon atom to which the nitroxide (doxyl) ring is linked (5DPC, 1-palmitoyl-2-stearoyl-(5-doxyl)-

DOI: 10.1021/acsomega.8b03395
ACS Omega 2019, 4, 5029−5037

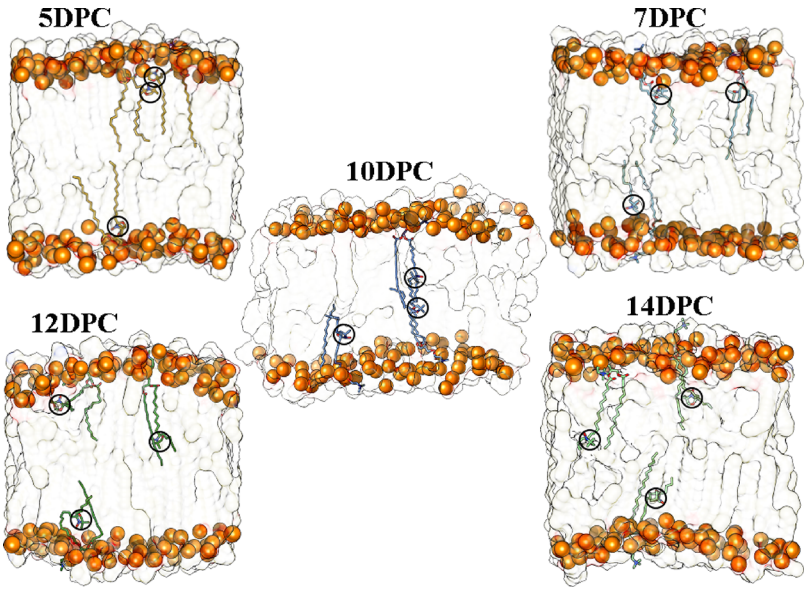

Figure 2. *n*DPC spin labels/egg−PC bilayers' snapshot of the MD simulation trajectory taken at the end of the simulations (t = 200 ns); water is omitted for clarity. For all the models, the lipids are represented as the transparent surface with the phosphorus atoms of the PC headgroups as orange spheres; *n*DPC molecules are shown as the classical stick representation in different colors hiding hydrogen for the purpose of clarity; the nitroxide ring is circled to highlight its position.

sn-glycero-3-phosphocholine in Scheme 2), as a representative example. In this work, besides 5DPC, we also used 7DPC, 10DPC, 12DPC, and 14DPC.

The overall box dimensions were 6.7 nm × 6.7 nm × 7.9 nm. The membrane composition is reported in Figure 1.

The simulation model systems were appropriately hydrated by adding water (4834 molecules). Initially, 2 mM NaCl was added to properly reproduce the experimental model. In order to check the role played by the salt in such a concentration on the bilayer structure and on the distribution of NOXs, a test calculation was carried out for the membrane model containing OG-NO either with or without 2 mM NaCl. These two simulations did not show any significant difference in the bilayer structure or the depth distribution of OG-NO; therefore, the calculations for all NOXs were carried out in the absence of NaCl (see the Supporting Information, Figure S4). Water−water interactions were modeled by using TIP3P,[21] whereas hydrogen bonds within the solvent molecules were constrained using the SHAKE algorithm.[22] Water and ions overlapping the membrane bilayer were removed before proceeding to system minimization.[23]

The starting pure egg−PC model was obtained by a membrane builder tool (Charmm-GUI, www.charmm-gui.org), minimized, and stabilized by a 10 ns equilibration by *NPT* MD simulation.[24] The system dimensions employed were chosen on the basis of literature reports, concerning the smallest representative size that can be used to accurately reproduce the occurring intermolecular interactions in lipid bilayers.[25−27] The GROMACS 5.0.4 suite of programs[28] was then used to perform all the simulations, by using the AMBER force field[29] (AMBERFF99SB, treating membrane with lipid11 parameter sets)[30−33] and extending its parameterization to provide the accurate description of large and flexible nitroxide free radicals; for this purpose, new atom types have been included, fitted on the basis of geometries, vibrational frequencies, and potential energy surfaces computed at the density functional theory level using B3LYP/6-311G** (Gaussian 09, Revision D.01)[24,34−37] and integrated into the FF parameters.

Going into details, the missing parameters were collected from those reported by Stendardo et al.[38] using the PBE0/N07D quantum mechanical calculations as the reference to extend the AMBER force field (FF99SB), particularly suitable to represent biological systems as membranes.[39,40] The derived parameters have also been tested to correctly predict the structural, dynamical, and spectroscopic features of the nitroxide radicals employed.[38]

The bilayer energy has been minimized under periodic box conditions, applied in all directions, using a neighbor searching grid type; the cutoff distance for the short-range neighbor list was set to 1.4 nm. Electrostatic interactions were taken into account by implementing a fast smooth particle-mesh Ewald algorithm[41−44] with a 1.4 nm distance for the Coulomb cutoff because this method is considered to be both efficient and accurate for the evaluation of long-range electrostatic interactions in large macromolecular systems.[45,46]

After geometry minimization, these systems underwent a 200 ns atomistic MD simulation using GROMACS 5.0 in the isothermal−isobaric (*NPT*) ensemble at 1 atm and 310 K (37 °C).[19] For all the MD trajectories, 2 ns of annealing simulations was carried out to gradually increase the temperature up to 310 K and then to generate atomic velocities; a weak temperature coupling (Berendsen thermostat), with a time constant of 1 ps, was applied to maintain the reference temperature (310 K) throughout the whole run; no water was observed inside the bilayer. At this point, 200 ns MD runs have been carried out for each of the built egg−PC bilayer/antioxidant systems. An accurate leap-frog stochastic dynamics integrator was used as the main run control option; we used a time step of 0.002 ps and the coordinates were written out every 10 ps, while energy data were collected every 2 ps. The first 2 ns MD simulation for each lipid system was carried out in the *NVT* ensemble using a Langevin thermostat, whereas the subsequent nanoseconds were carried out in the *NPT* ensemble (T = 310 K, P = 1 atm) using a Berendsen

DOI: 10.1021/acsomega.8b03395
ACS Omega 2019, 4, 5029−5037

thermostat and semi-isotropic pressure coupling. A time constant for coupling of 0.5 ps and an optimal compressibility for water of 4.5×10^{-5} bar^{-1} were used to obtain the best control on pressure. Computation of each MD trajectory was performed in parallel at a speed of 11 ns/day on a GALILEO IBM workstation (CINECA-HPC ISCRA project—see Acknowledgments). The achievement of a steady state for all of the simulated models was monitored through the molecular root-mean-square deviation (rmsd) values versus time.[47] Deviation was calculated as displacement with respect to the starting minimized structure.

MD Simulation Analyses. From the collected MD trajectories, the nitroxide N−O bond penetration depths within the bilayer have been determined. More in detail, the MD trajectories were collected until they reached equilibration, that is, until the equilibration trajectory achieved a full convergence of the system's dimensions and far over (Supporting Information—Figure S1).[47] The analysis of the simulations' trajectories was performed by means of the VMD and CHIMERA software.[48] We monitored the fluctuations of the nitroxide moiety and its dynamical behavior by evaluating the orientation of NO groups in the PC lipid system during MD simulations and calculated the mass density profile of nitroxide groups to show the volume probability distributions across the bilayer (Figure S2, Supporting Information). The final 20 ns of the MD trajectories were considered for subsequent analysis of the bilayer properties, after having verified the achievement of the steady-state condition for all the systems (see rmsd plot in Figure S3 reported in the Supporting Information and area-per-lipid fluctuation ΔA = 0.03 ± 0.01 nm^2); hence, the distance from the bilayer surface (R) of the nitroxide groups is referred to that state.

Structure of the NOXs. The NOXs considered for these calculations were those reported in Scheme 2:[13] they bear a pyrroline nitroxide moiety linked to a cholesterol unit (Chol-NO) or to a glycerol moiety; the latter can be esterified with one (OG-NO and OG(L)-NO) or two oleoyl units (DOG-NO and DOG(L)-NO). Two of these NOXs also contain a polar spacer group between the pyrroline and the glycerol moieties (OG(L)-NO and DOG(L)-NO).[13]

RESULTS AND DISCUSSION

Calibration and Validation of the Method by Using Commercial Spin-Labeled Phospholipids. The first batch of simulations was performed on an egg−PC bilayer containing commercially available phospholipid spin labels, *n*DPCs, which have been used as a "molecular ruler" for the estimation of the NOX penetration depth in the bilayer.[13,49,50] Snapshots taken at the end of the MD trajectories of the equilibrated simulated bilayers are reported in Figure 2, which also shows that the nitroxide rings attached to the carbon atoms that are more deeply located in the bilayer core possess a higher level of conformational flexibility, as expected.

In addition, the mass density profiles of water, of the phosphate groups, and of the different nitroxides (taken as the density of the N−O group—Supporting Information; Figure S2) have been computed. Moreover, at the spin label concentration used in our simulations, close to that used in the EPR experiments with *n*DPCs (3% of the total lipids), the overall perturbation induced on the bilayer structure was rather modest.

The average position of the nitroxide moieties within the bilayer followed the expected trend, showing a progressively increasing depth going from 5DPC to 14DPC. The increased lipid chain mobility as a function of depth, for those nitroxides located closer to the bilayer core, produces a corresponding broader density distribution, as qualitatively seen in Figure S2 (Supporting Information Section). Note that the *n*DPC molecules were located in both sides of the bilayer and no *flip-flop* motion was observed during the timeframe of the simulation.

The position of the nitroxide group of the *n*DPC phospholipids with respect to the membrane surface was initially validated by comparison with available data from the literature, referred to both computed and experimental data. The depth values were compared with the results obtained by MD simulations in a pure POPC membrane.[51] Although in that case the amount of spin labels was significantly higher (1:11 or 1:4 lipids: *n*DPC ratio) and the temperature was slightly different (303.15 K), the corresponding results are in good agreement with our simulations. In fact, as shown by the plot reported in Figure 3, the two sets of data are in general very close to the diagonal, which represents the perfect match

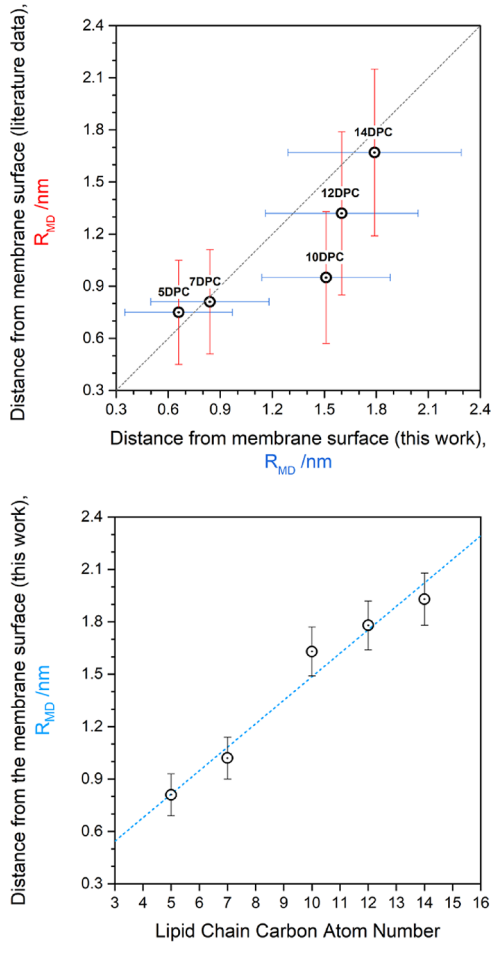

Figure 3. Top: Linear correlation plot of the distance of the nitroxide groups of *n*DPC from the membrane surface calculated in this work in egglike PC with respect to those obtained in POPC from ref 51. The colored bars represent the half-width of the calculated distribution in blue for the MD simulation of this work and in red for the literature data. The diagonal represents the best match between values. Bottom: Linear correlation plot of the calculated distances R of the nitroxide groups of *n*DPC from the membrane surface vs the number of the carbon atom of the lipid chain that bears the nitroxide moiety.

DOI: 10.1021/acsomega.8b03395
ACS Omega 2019, 4, 5029−5037

between the two sets of simulations; we draw the attention of the reader that the bars reported do not represent the uncertainty in the average position but the half-width of the calculated distributions.

The 10DPC molecule falls on the side of the linear correlation line, but this feature can be attributed to the different lipid compositions used in the simulations (egg−PC mixture vs pure POPC in ref 51): the nitroxide function of 10DPC is located in the middle of the lipid chain and can interact to a larger extent with the polyunsaturated moieties of the PLPC and SLPC lipids that we used in our model membrane. These interactions are not present in the set of simulations based on a pure POPC membrane,[51] and, as a consequence, the NO group of 10DPC, and to a lesser degree of 12DPC, is resulted, which is more deeply located in our MD trajectories. Additionally, we plotted the position of the *n*DPC nitroxide group versus the carbon number position with the corresponding error bars (bottom of Figure 3), where 10DPC only minimally deviates from the linearity.

The computed penetration depth was then correlated to the experimental parameter Φ (adimensional)[50,52−54] determined by EPR measurements.[13] Such a parameter is used to represent the insertion level of the nitroxide inside the membrane, and it is defined as the ratio between the collision frequency of the nitroxide with a water-soluble paramagnetic agent (NiEDDA or CROX) and that with a lipid-soluble paramagnetic agent (molecular oxygen).[49] The penetration depth parameter Φ for a paramagnetic molecule obtained from the EPR experiments can be converted in an absolute distance from the membrane surface (*R*, in nm) once a calibration curve is built.[55] We previously prepared such a curve using our values for *n*DPC nitroxides and the known depths of spin-labeled phospholipids, considering the X-ray/NMR data from Dalton et al.[56] (Supporting Information—Table S1); two linear regressions have been previously performed, one considering 5DPC[47] and one excluding it,[52] because in the latter case the linearity of the calibration curve largely increases. We point out that the apparent inversion of the insertion depth between 5DPC and 7DPC (Figure 4)[13,49] is not present in the calculation performed in this work nor can be found in the X-ray/NMR data, thus it must represent an artifact of the EPR method. We attribute the inversion to a deviation from the linearity of the oxygen/NiEDDA concentrations, as the method in use assumes a linear gradient of both species throughout the membrane. However, phospholipid membranes, especially in the headgroup region and immediately below, are far from being homogeneous, thus the distributions of oxygen and water-soluble molecules around positions 5 and 7 of the lipid chain might not be linear. An interesting development could be represented by a simulation of the *n*DPC lipids in the presence of explicit molecular oxygen and a water-soluble agent to correct the data obtained by the EPR methodology. However, although MD simulations of oxygen penetration are available,[57−60] a model that satisfactorily reproduces all parameters of oxygen partitioning is still under development.[61]

The simulations reported in this work allow the creation of a new curve obtained for a bilayer that closely matches the experimental conditions, allowing a better comparison for the penetration depth data of the NOXs (vide infra). Indeed, the previous calibration curves are based on X-ray/NMR data referring to the bilayers of DMPC, much shorter and with a different fluidity than those of POPC. This new calibration curve (R/nm = 0.54Φ + 0.44) is shown in Figure 4.

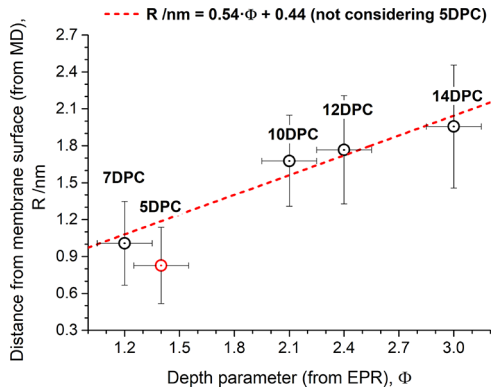

Figure 4. Membrane depth calibration curve to obtain the absolute membrane penetration depth from EPR experiments. The plot shows in the ordinate the distance from the membrane surface of the *n*DPC spin labels (*R*, in nanometers, the error is the half-width of the distribution), determined from the MD simulations of the present work, and in abscissa the experimental depth parameter (Φ, adimensional, the error is an estimate based on repeated experiments), determined from EPR experiments.[13] Note that the linear regression is performed by excluding 5DPC from the fitting for the reasons outlined in the text.

MD Simulations of Egg−PC Bilayers Containing the NOXs. A second set of simulations was carried out on an egg−PC bilayer in which the different NOXs (see Scheme 2) constitute 3% of the total phospholipids, and the positions of these nitroxides were calculated by MD. At the same time, the calibration curve (Φ vs position) discussed in the previous section (Figure 4) was exploited to obtain the absolute penetration depth (R_{EPR}) of the nitroxides from the experimental Φ parameters previously determined.[13] In our MD calculations, we evaluated the perturbation of the bilayer induced by the presence of NOXs and also found in this case that, at these concentrations, the perturbation of the bilayer is very modest.

The N−O penetration depths (R_{MD}) in the bilayer were obtained as the mass density profile averaged for the last 20 ns of MD simulations; the results are shown in Figure 5 and are characterized by typical Gaussian-like profiles with the maxima located at a different distance from the surface and different width. The calculated R_{MD} values are reported in Table 1, which can be directly compared to the corresponding R_{EPR} values. We observed a very good agreement between the experimental results and the simulations, showing in both cases that the penetration depth of the NOXs increases in the order Chol-NO ≪ DOG(L)-NO < DOG-NO < OG(L)-NO < OG-NO.

Major information on the localization and dynamics of nitroxides is given by the snapshots at the steady state, as shown in Figure 6. There, a large difference between Chol-NO and the other glycerolipid NOX behavior is evidenced: very likely, the rigid and almost planar core of Chol-NO keeps the molecule well-ordered in the bilayer with the nitroxide head pointing toward the water phase, locating itself in between the phosphate groups or immediately under them. Conversely, the glycerolipid NOXs are conformationally flexible and tend to push the nitroxide ring moiety toward the bilayer interior or parallel to the membrane surface. The observed nitroxide ring orientations in the MD simulations can be compared to the results previously obtained in DMPC/DHPC bicelles (magnetically aligned lipid bilayers).[13] Concerning Chol-NO, the

DOI: 10.1021/acsomega.8b03395
ACS Omega 2019, 4, 5029−5037

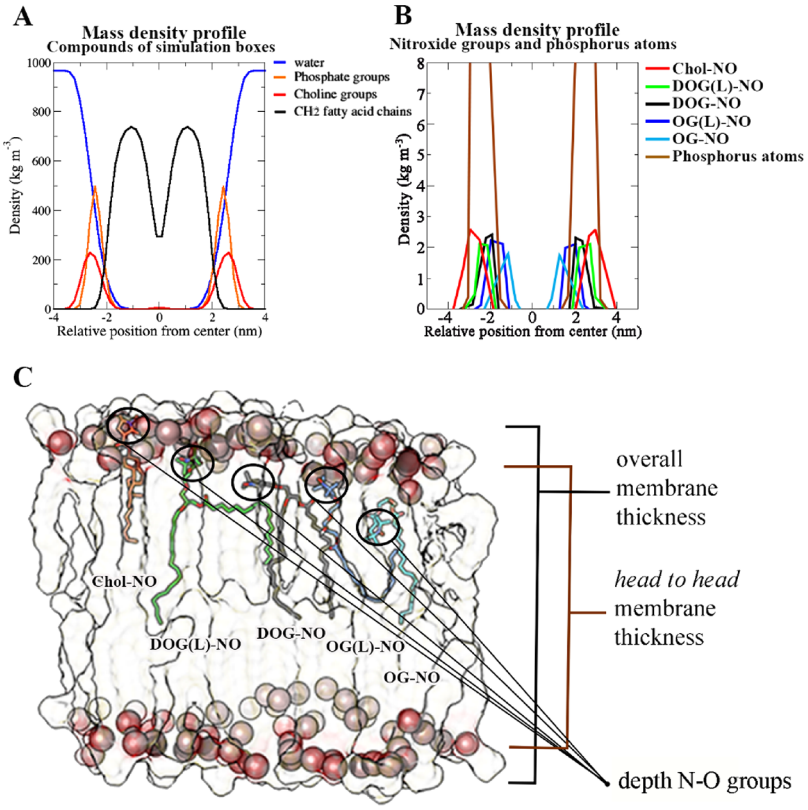

Figure 5. Mass density profiles within the simulation boxes (A) and focused on NOX nitroxide groups (B), with respect to the bilayer center (X = 0). In (C), NOXs/egg−PC bilayer models after MD stabilization showing the NO moiety depth inside the bilayer for each NOX. We reported the phosphorus atoms of the lipid phosphates as brown spheres and the compounds Chol-NO, DOG(L)-NO, DOG-NO, OG(L)-NO, and OG-NO as stick models in different colors. The N−O rings are circled to highlight their depth in the lipid membrane. The lipid matrix is represented as the transparent surface, and water and hydrogen atoms are omitted to improve the image clarity.

Table 1. Penetration Depth from the Bilayer Surface (R_{MD}) of NOX Nitroxide Groups in Egg−PC and Distance of the NO Group from the Bilayer Surface from EPR Data (R_{EPR}) Have Been Reported; the Uncertainty on R_{MD} Is the Half-Width of the Mass Density Profile, While the Uncertainty on R_{EPR} Is Obtained from the Error of the Linear Regression[a]

NOX	R_{MD}/nm	R_{EPR} (MD curve)/nm
Chol-NO	0.76 ± 0.12	0.82 ± 0.25
DOG(L)-NO	0.94 ± 0.12	1.20 ± 0.31
DOG-NO	1.10 ± 0.11	1.41 ± 0.35
OG(L)-NO	1.43 ± 0.12	1.47 ± 0.35
OG-NO	1.70 ± 0.11	1.57 ± 0.37

[a] R_{MD} values are averaged over the last 20 ns of the 200 ns MD simulations.

simulations of the EPR spectra indicated that the normal to the plane of the nitroxide ring is parallel to the membrane normal, as also shown by the MD simulations. An excellent agreement with the EPR data has also been found for the other NOXs, suggesting a larger tilt toward the bilayer core for the nitroxide head of OG-NO when compared to the other glycerolipids.

However, the position of the nitroxide groups with respect to the double bonds of the oleic/linoleic chains requires a separate discussion. As reported in Figure 7 (see also the Supporting Information), the oleic and linoleic double bonds, which represent the main site of lipid peroxidation initiation, are located at 1.59 nm from the phosphate head in the case of the C9 position, whereas the other linoleic double bond at C12 is located at 1.72 nm; the width (full width at half-height) of the distribution functions is about 0.6 nm. Because the N−O group represents the antioxidant active moiety of NOXs, the results of our simulations show that there is a definite overlap with the distribution function of the double bonds, in particular of the C9−C10 ones, with that of OG-NO and OG(L)-NO, a smaller overlap with the tails of the distributions for DOG-NO, DOG(L)-NO, while no overlap possibility is foreseen for Chol-NO. This result fully supports our supposition that the antioxidant activity of the glycerolipid-based NOXs is related to their ability to localize their N−O function nearby the membrane double bonds, while the antioxidant activity of Chol-NO should follow a different mechanism.[13]

CONCLUSIONS

In conclusion, the validation of the MD method presented in this study, carried out by combining experimental and in silico results, confirms the efficacy of the developed combined approach and opens new possibilities for the development of new nitroxide-based systems, targeting specifically the peroxidation processes in unsaturated membranes. This method allowed us to study the behavior of antioxidant molecules in bilayer systems, considering in detail the lipid matrix effect on the nitroxide moiety positioning. Overall, these results are particularly relevant for the future applications of this approach, which aims to tune the antioxidant properties of novel molecules in bilayers of different compositions, by

DOI: 10.1021/acsomega.8b03395
ACS Omega 2019, 4, 5029−5037

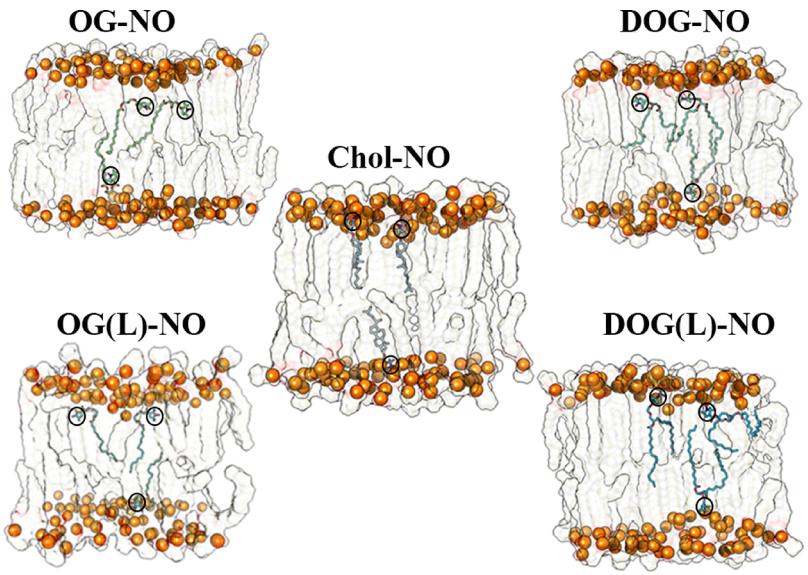

Figure 6. NOX egg−PC bilayers' snapshot of the MD simulation trajectory taken at the end of the simulations (t = 200 ns); water is omitted for clarity. For all the models, the lipids are represented as the transparent surface with the phosphorus atoms of the PC headgroups as orange spheres; NOX molecules are shown in classical stick representation in different colors hiding hydrogen for the purpose of clarity; the NO ring is circled to highlight its position.

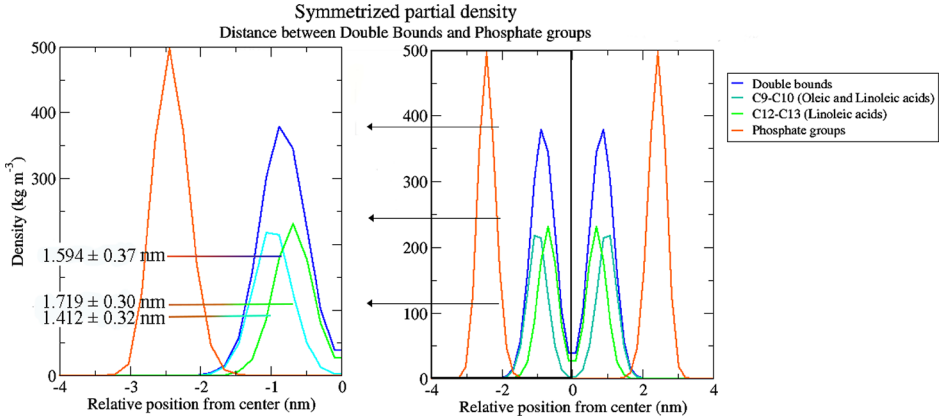

Figure 7. Density profile of the double bonds: the plot reports the carbon atoms C9−C10 for the oleic and linoleic acids and atoms C12−C13 for the linoleic fatty acid. The average distances of carbons C9−C10 from the phosphate groups are 1.401 ± 0.32 and 1.722 ± 0.31 nm for carbons C12−C13.

changing their shape and flexibility, in order to localize the active headgroup close to the main site of lipid peroxidation, that is, the unsaturated regions of the bilayers. The very good agreement found between MD and experimental results suggests that the method could also be successfully applied to nonparamagnetic antioxidants.

■ ASSOCIATED CONTENT

Supporting Information

The Supporting Information is available free of charge on the ACS Publications website at DOI: 10.1021/acsomega.8b03395.

Molecular Dynamics calculation details for liponitroxides *n*DPC: RMSD vs time for nDPCs (Figure S1); mass densities profiles for water, phosphate and nitroxide groups (Figure S2); RMSD of NOX molecules in the egg−PC membrane (Figure S3); effect of NaCl (2 mM) on the RSMD simulations of NOXs (Figure S4) (PDF)

■ AUTHOR INFORMATION

Corresponding Authors

*E-mail: r.galeazzi@univpm.it (R.G.).
*E-mail: antonio.barbon@unipd.it (A.B.).
*E-mail: p.stipa@univpm.it (P.S.).

ORCID

Antonio Barbon: 0000-0002-2009-5874
Marco Bortolus: 0000-0002-6033-6521
Pierluigi Stipa: 0000-0001-9024-0398

Notes

The authors declare no competing financial interest.

■ ACKNOWLEDGMENTS

ISCRA-CINECA is kindly acknowledged for providing granted projects allowing HPC calculation (ISCRA-call C 2015−2017) and Università Politecnica delle Marche for financial support. M.B. acknowledges the support of the CARIPARO foundation through the Starting Grant program.

DOI: 10.1021/acsomega.8b03395
ACS Omega 2019, 4, 5029−5037

REFERENCES

(1) Margaill, I.; Plotkine, M.; Lerouet, D. Antioxidant strategies in the treatment of stroke. *Free Radical Biol. Med.* **2005**, *39*, 429−443.

(2) Ribeiro, A.; Estanqueiro, M.; Oliveira, M.; Sousa Lobo, J. Main Benefits and Applicability of Plant Extracts in Skin Care Products. *Cosmetics* **2015**, *2*, 48−65.

(3) Finley, J. W.; Kong, A.-N.; Hintze, K. J.; Jeffery, E. H.; Ji, L. L.; Lei, X. G. Antioxidants in foods: state of the science important to the food industry. *J. Agric. Food Chem.* **2011**, *59*, 6837−6846.

(4) Pisoschi, A. M.; Pop, A. The role of antioxidants in the chemistry of oxidative stress: A review. *Eur. J. Med. Chem.* **2015**, *97*, 55−74.

(5) Damiani, E.; Astolfi, P.; Carloni, P.; Stipa, P.; Greci, L. Antioxidants: how they work. In *Oxidants in Biology: a Question of Balance*; Valacchi, G., Davis, P., Eds.; Springer (De), 2008.

(6) Krishna, M. C.; Samuni, A. [59] Nitroxides as antioxidants. *Methods Enzymol.* **1994**, *234*, 580−589.

(7) Lewandowski, M.; Gwozdzinski, K. Nitroxides as Antioxidants and Anticancer Drugs. *Int. J. Mol. Sci.* **2017**, *18*, 2490.

(8) Astolfi, P.; Carloni, P.; Marini, M. G.; Mobbili, G.; Pisani, M.; Stipa, P. Benzoxazinic nitrones and nitroxides as possible antioxidants in biological systems. *RSC Adv.* **2013**, *3*, 22023−22030.

(9) Samuni, A.; Goldstein, S.; Russo, A.; Mitchell, J. B.; Krishna, M. C.; Neta, P. Kinetics and Mechanism of Hydroxyl Radical and OH-Adduct Radical Reactions with Nitroxides and with Their Hydroxylamines. *J. Am. Chem. Soc.* **2002**, *124*, 8719−8724.

(10) Krishna, M. C.; Grahame, D. A.; Samuni, A.; Mitchell, J. B.; Russo, A. Oxoammonium cation intermediate in the nitroxide-catalyzed dismutation of superoxide. *Proc. Natl. Acad. Sci. U.S.A.* **1992**, *89*, 5537−5541.

(11) Bar-On, P.; Mohsen, M.; Zhang, R.; Feigin, E.; Chevion, M.; Samuni, A. Kinetics of Nitroxide Reaction with Iron(II). *J. Am. Chem. Soc.* **1999**, *121*, 8070−8073.

(12) Goldstein, S.; Rosen, G. M.; Russo, A.; Samuni, A. Kinetics of Spin Trapping Superoxide, Hydroxyl, and Aliphatic Radicals by Cyclic Nitrones. *J. Phys. Chem. A* **2004**, *108*, 6679−6685.

(13) Mobbili, G.; Crucianelli, E.; Barbon, A.; Marcaccio, M.; Pisani, M.; Dalzini, A.; Ussano, E.; Bortolus, M.; Stipa, P.; Astolfi, P. Liponitroxides: EPR study and their efficacy as antioxidants in lipid membranes. *RSC Adv.* **2015**, *5*, 98955−98966.

(14) Galeazzi, R.; Laudadio, E.; Massaccesi, L. *Recent advances in Computational Simulations of Lipid Bilayer Based Molecular Systems Frontiers in Computational Chemistry*; Ul-Haq, Z., Madura, J.-D., Eds.; Bentham Science, 2015; Vol. *2*, pp 326−388.

(15) Abraham, M. J.; Murtola, T.; Schulz, R.; Páll, S.; Smith, J. C.; Hess, B.; Lindahl, E. GROMACS: High performance molecular simulations through multi-level parallelism from laptops to supercomputers. *SoftwareX* **2015**, *1−2*, 19−25.

(16) van Meer, G.; Voelker, D. R.; Feigenson, G. W. Membrane lipids: where they are and how they behave. *Nat. Rev. Mol. Cell Biol.* **2008**, *9*, 112−124.

(17) Laudadio, E.; Mobbili, G.; Minnelli, C.; Massaccesi, L.; Galeazzi, R. Salts influence cathechins and flavonoids encapsulation in liposomes: a molecular dynamics investigation. *Mol. Inf.* **2017**, *36*, 1700059.

(18) Galeazzi, R.; Mobbili, G.; Laudadio, E.; Minnelli, C.; Amici, A.; Massaccesi, L. Liposomial formulations for an efficient encapsulation Epigallocatechin-3-gallate: an in silico/experimental approach. *Molecules* **2018**, *23*, 441.

(19) Galeazzi, R.; Bruni, P.; Crucianelli, E.; Laudadio, E.; Marini, M.; Massaccesi, L.; Mobbili, G.; Pisani, M. Liposome-based gene delivery systems containing a steroid derivative: computational and small angle X-ray diffraction study. *RSC Adv.* **2015**, *5*, 54070−54078.

(20) Sigma-Aldrich, from egg yolk, type XVI-E, ≥99% (TLC), lyophilized powder prepared by a modification of the procedure of Singleton, W. S., et al., *J. Am. Oil Chem. Soc.,* **1965**, *42,* 53.

(21) Jorgensen, W. L.; Chandrasekhar, J.; Madura, J. D.; Impey, R. W.; Klein, M. L. Comparison of simple potential functions for simulating liquid water. *J. Chem. Phys.* **1983**, *79*, 926−935.

(22) Ryckaert, J.-P.; Ciccotti, G.; Berendsen, H. J. C. Numerical integration of the Cartesian Equations of Motion of a System with Constraints: Molecular Dynamics of n-Alkanes. *J. Comput. Phys.* **1977**, *23*, 321−341.

(23) Soper, A. K.; Bruni, F.; Ricci, M. A. Site-site pair correlation functions of water from 25 to 400 °C: Revised analysis of new and old diffraction data. *J. Chem. Phys.* **1997**, *106*, 247−254.

(24) Klauda, J. B.; Venable, R. M.; Freites, J. A.; O'Connor, J. W.; Tobias, D. J.; Mondragon-Ramirez, C.; Vorobyov, I.; MacKerell, A. D., Jr.; Pastor, R. W. Update of the CHARMM all-atom additive force field for lipids: validation on six lipid types. *J. Phys. Chem. B* **2010**, *114*, 7830−7843.

(25) Villanueva, D. Y.; Lim, J. B.; Klauda, J. B. Influence of Ester-Modified Lipids on Bilayer Structure. *Langmuir* **2013**, *29*, 14196−14203.

(26) Jo, S.; Rui, H.; Lim, J. B.; Klauda, J. B.; Im, W. Cholesterol Flip-Flop: Insights From Free Energy Simulation Studies. *J. Phys. Chem. B* **2010**, *114*, 13342−13348.

(27) Klauda, J. B.; Brooks, B. R.; Pastor, R. W. Dynamical Motions of Lipids and a Finite Size Effect in Simulations of Bilayers. *J. Chem. Phys.* **2006**, *125*, 144710.

(28) Case, D. A.; Cheatham, T. E., 3rd; Darden, T.; Gohlke, H.; Luo, R.; Merz, K. M., Jr.; Onufriev, A.; Simmerling, C.; Wang, B.; Woods, R. J. The Amber biomolecular simulation programs. *J. Comput. Chem.* **2005**, *26*, 1668−1688.

(29) Weiner, S. J.; Kollman, P. A.; Case, D. A.; Singh, U. C.; Ghio, C.; Alagona, G.; Profeta, S.; Weiner, P., Jr. A new force field for molecular mechanical simulation of nucleic acids and proteins. *J. Am. Chem. Soc.* **1984**, *106*, 765−784.

(30) Lyu, Y.; Xiang, N.; Zhu, X.; Narsimhan, G. Potential of mean force for insertion of antimicrobial peptide melittin into a pore in mixed DOPC/DOPG lipid bilayer by molecular dynamics simulation. *J. Chem. Phys.* **2017**, *146*, 155101.

(31) Thanki, K.; Prajapati, R.; Sangamwar, A. T.; Jain, S. Long chain fatty acid conjugation remarkably decreases the aggregation induced toxicity of Amphotericin B. *Int. J. Pharm.* **2018**, *544*, 1−13.

(32) Sierra, M. B.; Alarcón, L.; Gerbino, D.; Pedroni, V. I.; Buffo, F. E.; Morini, M. A. Effects of hydroxy-xanthones on dipalmitoylphosphatidylcholine lipid bilayers: A theoretical and experimental study. *Chem. Phys. Lipids* **2017**, *206*, 1−8.

(33) Laudadio, E.; Mobbili, G.; Minnelli, C.; Massaccesi, L.; Galeazzi, R. Salts Influence Cathechins and Flavonoids Encapsulation in Liposomes: A Molecular Dynamics Investigation. *Mol. Inf.* **2017**, *36*, 1700059.

(34) Lee, C.; Yang, W.; Parr, R. G. Development of the Colle-Salvetti correlation-energy formula into a functional of the electron density. *Phys. Rev. B: Condens. Matter Mater. Phys.* **1988**, *37*, 785−789.

(35) Vosko, S. H.; Wilk, L.; Nusair, M. Accurate spindependent electron liquid correlation energies for local spin density calculations: a critical analysis. *Can. J. Phys.* **1980**, *58*, 1200−1211.

(36) Stephens, P. J.; Devlin, F. J.; Chabalowski, C. F.; Frisch, M. J. Ab Initio Calculation of Vibrational Absorption and Circular Dichroism Spectra Using Density Functional Force Fields. *J. Phys. Chem.* **1994**, *98*, 11623−11627.

(37) Becke, A. D. Density-functional thermochemistry. III. The role of exact exchange. *J. Chem. Phys.* **1993**, *98*, 5648−5652.

(38) Stendardo, E.; Pedone, A.; Cimino, P.; Cristina Menziani, M.; Crescenzi, O.; Barone, V. Extension of the AMBER Force-Field for the Study of Large Nitroxides in Condensed Phases: An ab initio Parameterization. *Phys. Chem. Chem. Phys.* **2010**, *12*, 11697−11709.

(39) Barone, V.; Bloino, J.; Biczysko, M. Validation of the DFT/N07D computational model on the magnetic, vibrational and electronic properties of vinyl radical. *Phys. Chem. Chem. Phys.* **2010**, *12*, 1092−1101.

(40) Hornak, V.; Abel, R.; Okur, A.; Strockbine, B.; Roitberg, A.; Simmerling, C. Comparison of multiple Amber force fields and development of improved protein backbone parameters. *Proteins* **2006**, *65*, 712−725.

DOI: 10.1021/acsomega.8b03395
ACS Omega 2019, 4, 5029−5037

(41) Darden, T.; York, D.; Pedersen, L. Particle mesh Ewald: An N·log(N) method for Ewald sums in large systems. *J. Chem. Phys.* **1993**, *98*, 10089−10092.
(42) Ewald, P. P. Die Berechnung optischer und elektrostatischer Gitterpotentiale. *Ann. Phys.* **1921**, *369*, 253−287.
(43) Hockney, R. W.; Eastwood, J. W. *Computer Simulation Using Particles*; McGraw-Hill: New York, 1988.
(44) Pronk, S.; Páll, S.; Schulz, R.; Larsson, P.; Bjelkmar, P.; Apostolov, R.; Shirts, M. R.; Smith, J. C.; Kasson, P. M.; van der Spoel, D.; Hess, B.; Lindahl, E. GROMACS 4.5: a high-throughput and highly parallel open source molecular simulation toolkit. *Bioinformatics* **2013**, *29*, 845−854.
(45) Galeazzi, R. Molecular Dynamics as a Tool in Rational Drug Design: Current Status and Some Major Applications. *Curr. Comput.-Aided Drug Des.* **2009**, *5*, 225−240.
(46) Eastwood, J. W.; Hockney, R. W.; Lawrence, D. N. P3M3DP-The three-dimensional periodic particle-particle/ particle-mesh program. *Comput. Phys. Commun.* **1980**, *19*, 215−261.
(47) Porasso, R. D.; Cascales, J. J. L. A criterion to identify the equilibration time in lipid bilayer simulations. *Pap. Phys.* **2012**, *4*, 040005.
(48) Pettersen, E. F.; Goddard, T. D.; Huang, C. C.; Couch, G. S.; Greenblatt, D. M.; Meng, E. C.; Ferrin, T. E. UCSF Chimera?A visualization system for exploratory research and analysis. *J. Comput. Chem.* **2004**, *25*, 1605−1612.
(49) Altenbach, C.; Greenhalgh, D. A.; Khorana, H. G.; Hubbell, W. L. A collision gradient method to determine the immersion depth of nitroxides in lipid bilayers: application to spin-labeled mutants of bacteriorhodopsin. *Proc. Natl. Acad. Sci. U.S.A.* **1994**, *91*, 1667−1671.
(50) Bortolus, M.; Dalzini, A.; Formaggio, F.; Toniolo, C.; Gobbo, M.; Maniero, A. L. An EPR study of ampullosporin A, a medium-length peptaibiotic, in bicelles and vesicles. *Phys. Chem. Chem. Phys.* **2016**, *18*, 749−760.
(51) Kyrychenko, A.; Ladokhin, A. S. Molecular Dynamics Simulations of Depth Distribution of Spin-Labeled Phospholipids within Lipid Bilayer. *J. Phys. Chem. B* **2013**, *117*, 5875−5885.
(52) Bortolus, M.; Dalzini, A.; Toniolo, C.; Hahm, K.-S.; Maniero, A. L. Interaction of hydrophobic and amphipathic antimicrobial peptides with lipid bicelles. *J. Pept. Sci.* **2014**, *20*, 517−525.
(53) Bortolus, M.; De Zotti, M.; Formaggio, F.; Maniero, A. L. Alamethicin in bicelles: Orientation, aggregation, and bilayer modification as a function of peptide concentration. *Biochim. Biophys. Acta, Biomembr.* **2013**, *1828*, 2620−2627.
(54) Bortolus, M.; Parisio, G.; Maniero, A. L.; Ferrarini, A. Monomeric fullerenes in lipid membranes: effects of molecular shape and polarity. *Langmuir* **2011**, *27*, 12560−12568.
(55) Bortolus, M.; Dalzini, A.; Maniero, A. L.; Panighel, G.; Siano, A.; Toniolo, C.; De Zotti, M.; Formaggio, F. Insights into peptide-membrane interactions of newly synthesized, nitroxide-containing analogs of the peptaibiotic trichogin GAIV using EPR. *Biopolymers* **2017**, *108*, No. e22913.
(56) Dalton, L. A.; McIntyre, J. O.; Fleischer, S. Distance estimate of the active center of D-.beta.-hydroxybutyrate dehydrogenase from the membrane surface. *Biochemistry* **1987**, *26*, 2117−2130.
(57) Marrink, S. J.; Berendsen, H. J. C. Permeation process of small molecules across lipid membranes studied by molecular dynamics simulations. *J. Phys. Chem.* **1996**, *100*, 16729−16738.
(58) Shinoda, W.; Mikami, M.; Baba, T.; Hato, M. Molecular dynamics study on the effects of chain branching on the physical properties of lipid bilayers: 2. Permeability. *J. Phys. Chem. B* **2004**, *108*, 9346−9356.
(59) Sugii, T.; Takagi, S.; Matsumoto, Y. A molecular-dynamics study of lipid bilayers: effects of the hydrocarbon chain length on permeability. *J. Chem. Phys.* **2005**, *123*, 184714.
(60) Holland, B. W.; Berry, M. D.; Gray, C. G.; Tomberli, B. A Permeability Study of O_2 and the Trace Amine p-Tyramine through Model Phosphatidylcholine. *PLoS One* **2015**, *10*, No. e0122468.
(61) Javanainen, M.; Vattulainen, I.; Monticelli, L. On Atomistic Models for Molecular Oxygen. *J. Phys. Chem. B* **2017**, *121*, 518−528.

DOI: 10.1021/acsomega.8b03395
ACS Omega 2019, 4, 5029−5037